J|A|C|S
ARTICLES

Published on Web 03/04/2010

# Efficient Photoinduced Electron Transfer in a Porphyrin Tripod−Fullerene Supramolecular Complex via $\pi-\pi$ Interactions in Nonpolar Media

Atsuro Takai,[†] Mohammed Chkounda,[‡] Antoine Eggenspiller,[‡] Claude P. Gros,[‡] Mohammed Lachkar,[§] Jean-Michel Barbe,*[,‡] and Shunichi Fukuzumi*[,†,||]

*Department of Material and Life Science, Division of Advanced Science and Biotechnology, Graduate School of Engineering, Osaka University, SORST, Japan Science and Technology Agency (JST), Suita, Osaka 565-0871, Japan, ICMUB, UMR CNRS 5260, Université de Bourgogne, 9 Avenue Alain Savary, BP 47870, 21078 Dijon Cedex, France, Université Sidi Mohamed Ben Abdellah, Faculté des Sciences Dhar El Mahraz, Laboratoire d'Ingénierie des Matériaux Organométalliques et Moléculaires "L.I.M.O.M.", Département de Chimie, B.P. 1796 (Atlas), 30000 Fès, Maroc, Department of Bioinspired Science, Ewha Womans University, Seoul 120-750, Korea*

Received January 9, 2010; E-mail: fukuzumi@chem.eng.osaka-u.ac.jp; Jean-Michel.Barbe@u-bourgogne.fr

***Abstract:*** A novel porphyrin tripod ($TPZn_3$) was synthesized via "click chemistry". Three porphyrin moieties of $TPZn_3$ are geometrically close and linked by a flexible linker. The electron-transfer oxidation of $TPZn_3$ results in intramolecular $\pi$-dimer formation between porphyrin moieties as indicated by electrochemical, vis−NIR, and ESR measurements. The cyclic voltammogram of $TPZn_3$ exhibited stepwise one-electron oxidation processes of three porphyrin moieties in the range from 0.58 to 0.73 V (vs SCE in $CH_2Cl_2$). When $TPZn_3$ was oxidized by tris(2,2′-bipyridyl)-ruthenium(III) ($[Ru(bpy)_3]^{3+}$), the oxidized species $(TPZn_3)^{n+}$ ($0 < n \leq 3$) exhibited a charge resonance band in the NIR region due to the $\pi$-dimer formation between porphyrin moieties. A supramolecular electron donor−acceptor system was also constructed using $TPZn_3$. The flexible conformation of $TPZn_3$ makes it possible to capture a fullerene derivative containing a pyridine moiety ($PyC_{60}$) inside the cavity by $\pi-\pi$ interactions as well as the coordination bond between $Zn^{2+}$ and the pyridine moiety. The formation of a 1:1 supramolecular complex of $TPZn_3$ with $PyC_{60}$ ($TPZn_3-PyC_{60}$) was indicated in the UV−vis and $^1H$ NMR spectra in nonpolar solvents. The association constant of $TPZn_3$ with $PyC_{60}$ ($1.1 \times 10^5\ M^{-1}$ in toluene) is much larger as compared with those of the corresponding monomer (MPZn) and dimer porphyrin ($DPZn_2$). The dynamics of photoinduced electron transfer from the singlet excited state of $TPZn_3$ to $PyC_{60}$ was examined by laser flash photolysis measurements. The efficient intracomplex photoinduced electron transfer in $TPZn_3-PyC_{60}$ occurred in nonpolar solvents, resulting from the $\pi-\pi$ interactions between the porphyrin and fullerene moieties, together with intramolecular $\pi$-bond formation between the porphyrin radical cation and the neutral porphyrin in $TPZn_3^{\bullet+}$.

## Introduction

In the initial photosynthetic process, the light energy collected by chlorophyll assemblies, light-harvesting antenna, is funneled into photosynthetic reaction center. Then, the multistep electron-transfer reactions occur following the excitation of the chlorophyll dimer, the so-called "special pair", to attain the long-lived charge separated state with nearly 100% quantum yield.[1] In this process, photosynthetic components are maintained by noncovalent interactions in relatively nonpolar membrane proteins. Thus, it is quite beneficial to utilize noncovalent interaction in order to construct electron donor−acceptor composites from the viewpoint of mimicking the biological photosystems in addition to easier accessibility as compared to covalently linked electron donor−acceptor ensembles. Extensive efforts have so far been devoted toward the design of such supramolecular electron donor−acceptor composites.[2−16] Porphyrins are particularly

[†] Osaka University.
[‡] Université de Bourgogne.
[§] Université Sidi Mohamed Ben Abdellah.
[||] Ewha Womans University.

(1) (a) Hoff, A. J.; Deisenhofer, J. *Phys. Rep.* **1997**, *287*, 1. (b) *Anoxygenic Photosynthetic Bacteria*; Blankenship, R. E., Madigan, M. T., Bauer, C. E., Eds.; Kluwer Academic Publishers: Dordrecht, The Netherlands, 1995.
(2) Wasielewski, M. R. *Chem. Rev.* **1992**, *92*, 435.
(3) (a) Sessler, J. L.; Lawrence, C. M.; Jayawickramarajah, J. *Chem. Soc. Rev.* **2007**, *36*, 314. (b) Sessler, J. L.; Wang, B.; Harriman, A. *J. Am. Chem. Soc.* **1993**, *115*, 10418.
(4) Aoyama, Y.; Asakawa, M.; Matsui, Y.; Ogoshi, H. *J. Am. Chem. Soc.* **1991**, *113*, 6233.
(5) Kuramochi, Y.; Satake, A.; Itou, M.; Ogawa, K.; Araki, Y.; Ito, O.; Kobuke, Y. *Chem.−Eur. J.* **2008**, *14*, 2827.
(6) Wang, Y. B.; Lin, Z. Y. *J. Am. Chem. Soc.* **2003**, *125*, 6072.
(7) Gayathri, S. S.; Wielopolski, M.; Perez, E. M.; Fernandez, G.; Sanchez, L.; Viruela, R.; Orti, E.; Guldi, D. M.; Martin, N. *Angew. Chem., Int. Ed.* **2009**, *48*, 815.
(8) (a) D'Souza, F.; Deviprasad, G. R.; Zandler, M. E.; Hoang, V. T.; Klykov, A.; VanStipdonk, M.; Perera, A.; El-Khouly, M. E.; Fujitsuka, M.; Ito, O. *J. Phys. Chem. A* **2002**, *106*, 3243. (b) D'Souza, F.; Deviprasad, G. R.; El-Khouly, M. E.; Fujitsuka, M.; Ito, O. *J. Am. Chem. Soc.* **2001**, *123*, 5277. (c) D'Souza, F.; Ito, O. *Coord. Chem. Rev.* **2005**, *249*, 1410.

 © 2010 American Chemical Society 

attractive building blocks for construction of supramolecular electron donor−acceptor composites using $\pi-\pi$ interaction due to their excellent photophysical and electron-transfer properties.[2−10,12a,16,17] However, noncovalent binding between highly $\pi$-conjugated compounds such as porphyrins and fullerenes is not strong enough in polar solvents which are generally used for studies on photoinduced electron-transfer reactions.[9a,12a,18−21] Thus, two-point binding sites have been introduced for porphyrin−fullerene systems:[11−13] e.g., axial coordination (zinc ion of porphyrin and pyridyl or imidazole moieties of fullerene derivatives) and ionic interaction (cation−crown ether complex).[12,13] Porphyrin dimers have also been employed to enhance the $\pi-\pi$ interactions with electron acceptors.[14,22]

*Scheme 1*

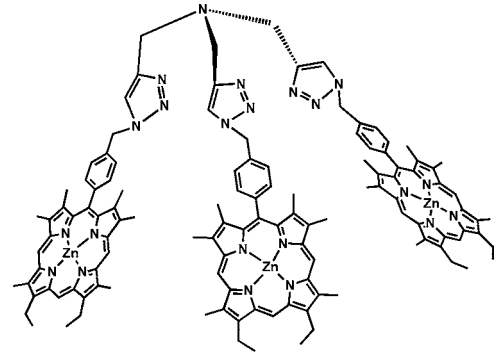

**$TPZn_3$**

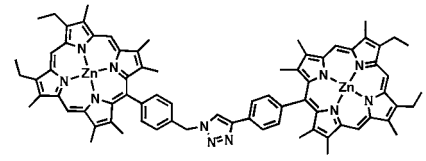

**$DPZn_2$**

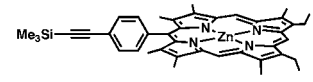


**MPZn**

Multiple porphyrin assemblies, such as the light-harvesting antenna and the special pair, are indispensable components for photosynthetic systems in which $\pi-\pi$ interaction between macrocyclic rings plays important roles in efficient energy transfer and electron transfer.[23] In this context, we reported that the enhanced electron-transfer properties of cofacial porphyrin dimers, in relation with the important role of the special pair in the photosynthetic reaction center, results from the smaller reorganization energy ($\lambda$) together with the larger driving force of the photoinduced electron transfer due to the $\pi$-electron delocalization in the dimer radical cations.[24] However, there is no example for investigations on the electron-transfer properties of multiporphyrins focusing on the $\pi$-bond formation among the oxidized multiporphyrins or on photoinduced electron transfer in supramolecular complexes of multiporphyrins with electron acceptors in nonpolar media.

We report herein the design and synthesis of a novel porphyrin trimer $TPZn_3$ (shown in Scheme 1), its electron-transfer properties, and construction of a highly organized

(9) (a) Fukuzumi, S. *Pure Appl. Chem.* **2007**, *79*, 981. (b) Fukuzumi, S.; Kojima, T. *J. Mater. Chem.* **2008**, *18*, 1427.
(10) (a) Hasobe, T.; Saito, K.; Kamat, P. V.; Troiani, V.; Qiu, H.; Solladié, N.; Kim, K. S.; Park, J. K.; Kim, D.; D'Souza, F.; Fukuzumi, S. *J. Mater. Chem.* **2007**, *17*, 4160. (b) Hasobe, T.; Kamat, P. V.; Troiani, V.; Solladié, N.; Ahn, T. K.; Kim, S. K.; Kim, D.; Kongkanand, A.; Kuwabata, S.; Fukuzumi, S. *J. Phys. Chem. B* **2005**, *109*, 19.
(11) (a) D'Souza, F.; Gadde, S.; Zandler, M. E.; Itou, M.; Araki, Y.; Ito, O. *Chem. Commun.* **2004**, 2276. (b) Hill, J. P.; Sandanayaka, A. S. D.; McCarty, A. L.; Karr, P. A.; Zandler, M. E.; Charvet, R.; Ariga, K.; Araki, Y.; Ito, O.; D'Souza, F. *Eur. J. Org. Chem.* **2006**, 595. (c) Gadde, S.; Islam, D. M. S.; Wijesinghe, C. A.; Subbaiyan, N. K.; Zandler, M. E.; Araki, Y.; Ito, O.; D'Souza, F. *J. Phys. Chem. C* **2007**, *111*, 12500.
(12) (a) D'Souza, F.; Ito, O. *Chem. Commun.* **2009**, 4913. (b) D'Souza, F.; Chitta, R.; Gadde, S.; Zandler, M. E.; McCarty, A. L.; Sandanayaka, A. S.; Araki, Y.; Ito, O. *Chem.−Eur. J.* **2005**, *11*, 4416.
(13) (a) D'Souza, F.; Chitta, R.; Gadde, S.; Rogers, L. M.; Karr, P. A.; Zandler, M. E.; Sandanayaka, A. S.; Araki, Y.; Ito, O. *Chem.−Eur. J.* **2007**, *13*, 916. (b) D'Souza, F.; Chitta, R.; Gadde, S.; Zandler, M. E.; Sandanayaka, A. S. D.; Araki, Y.; Ito, O. *Chem. Commun.* **2005**, 1279. (c) D'Souza, F.; Maligaspe, E.; Ohkubo, K.; Zandler, M. E.; Subbaiyan, N. K.; Fukuzumi, S. *J. Am. Chem. Soc.* **2009**, *131*, 8787.
(14) Tanaka, M.; Ohkubo, K.; Gros, C. P.; Guilard, R.; Fukuzumi, S. *J. Am. Chem. Soc.* **2006**, *128*, 14625.
(15) Kojima, T.; Honda, T.; Ohkubo, K.; Shiro, M.; Kusukawa, T.; Fukuda, T.; Kobayashi, N.; Fukuzumi, S. *Angew. Chem., Int. Ed.* **2008**, *47*, 6712.
(16) Straight, S. D.; Kodis, G.; Terazono, Y.; Hambourger, M.; Moore, T. A.; Moore, A. L.; Gust, D. *Nat. Nanotechnol.* **2008**, *3*, 280.
(17) Schlundt, S.; Kuzmanich, G.; Spanig, F.; de Miguel Rojas, G.; Kovacs, C.; Garcia-Garibay, M. A.; Guldi, D. M.; Hirsch, A. *Chem.−Eur. J.* **2009**, *15*, 12223.
(18) (a) *Electron Transfer in Chemistry*; Balzani, V., Ed.; Wiley-VCH: Weinheim, Germany, 2001. (b) Gust, D.; Moore, T. A. In *The Porphyrin Handbook*; Kadish, K. M., Smith, K. M., Guilard, R., Eds.; Academic Press: San Diego, CA, 2000; Vol. 8, pp 153−190.
(19) Imahori, H.; El-Khouly, M. E.; Fujitsuka, M.; Ito, O.; Sakata, Y.; Fukuzumi, S. *J. Phys. Chem. A* **2001**, *105*, 325.
(20) (a) Osuka, A.; Kobayashi, F.; Maruyama, K.; Mataga, N.; Asahi, T.; Okada, T.; Yamazaki, I.; Nishimura, Y. *Chem. Phys. Lett.* **1993**, *201*, 223. (b) Palacios, R. E.; Kodis, G.; Gould, S. L.; de la Garza, L.; Brune, A.; Gust, D.; Moore, T. A.; Moore, A. L. *ChemPhysChem* **2005**, *6*, 2359. (c) Linke, M.; Chambron, J.-C.; Heitz, V.; Sauvage, S. P.; Encinas, S.; Barigelletti, F.; Flamigni, L. *J. Am. Chem. Soc.* **2000**, *122*, 11834. (d) Luo, C.; Guldi, D. M.; Imahori, H.; Tamaki, K.; Sakata, K. *J. Am. Chem. Soc.* **2000**, *122*, 6535. (e) Fazio, M. A.; Durandin, A.; Tkachenko, N. V.; Niemi, M.; Lemmetyinen, H.; Schuster, D. I. *Chem.−Eur. J.* **2009**, *15*, 7698. (f) Tong, L. H.; Wietor, J. L.; Clegg, W.; Raithby, P. R.; Pascu, S. I.; Sanders, J. K. *Chem.−Eur. J.* **2008**, *14*, 3035.
(21) (a) Fukuzumi, S.; Ohkubo, K.; E, W.; Ou, Z.; Shao, J.; Kadish, K. M.; Hutchison, J. A.; Ghiggino, K. P.; Sintic, P. J.; Crossley, M. J. *J. Am. Chem. Soc.* **2003**, *125*, 14984. (b) D'Souza, F.; Chitta, R.; Ohkubo, K.; Tasior, M.; Subbaiyan, N. K.; Zandler, M. E.; Rogacki, M. K.; Gryko, D. T.; Fukuzumi, S. *J. Am. Chem. Soc.* **2008**, *130*, 14263. (c) Fukuzumi, S.; Hasobe, T.; Ohkubo, K.; Crossley, M. J.; Kamat, P. V.; Imahori, H. *J. Porphyrins Phthalocyanines* **2004**, *8*, 191. (d) Ohkubo, K.; Sintic, P. J.; Tkachenko, N. V.; Lemmetyinen, H.; E, W. B.; Ou, Z. P.; Shao, J. G.; Kadish, K. M.; Crossley, M. J.; Fukuzumi, S. *Chem. Phys.* **2006**, *326*, 3.
(22) (a) Tashiro, K.; Aida, T.; Zheng, J.-Y.; Kinbara, K.; Saigo, K.; Sakamoto, S.; Yamaguchi, K. *J. Am. Chem. Soc.* **1999**, *121*, 9477. (b) Shoji, Y.; Tashiro, K.; Aida, T. *J. Am. Chem. Soc.* **2004**, *126*, 6570.
(23) (a) Pullerits, T.; Sundstrom, V. *Acc. Chem. Res.* **1996**, *29*, 381. (b) Jordan, P.; Fromme, P.; Witt, H. T.; Klukas, O.; Saenger, W.; Krauss, N. *Nature* **2001**, *411*, 909. (c) Ferreira, K. N.; Iverson, T. M.; Maghlaoui, K.; Barber, J.; Iwata, S. *Science* **2004**, *303*, 1831. (d) Liu, Z. F.; Yan, H. C.; Wang, K. B.; Kuang, T. Y.; Zhang, J. P.; Gui, L. L.; An, X. M.; Chang, W. R. *Nature* **2004**, *428*, 287. (e) Pascal, A. A.; Liu, Z. F.; Broess, K.; van Oort, B.; van Amerongen, H.; Wang, C.; Horton, P.; Robert, B.; Chang, W. R.; Ruban, A. *Nature* **2005**, *436*, 134. (f) Loll, B.; Kern, J.; Saenger, W.; Zouni, A.; Biesiadka, J. *Nature* **2005**, *438*, 1040. (g) Amunts, A.; Drory, O.; Nelson, N. *Nature* **2007**, *447*, 58.
(24) Takai, A.; Gros, C. P.; Barbe, J.-M.; Guilard, R.; Fukuzumi, S. *Chem.−Eur. J.* **2009**, *15*, 3110.

***Scheme 2***

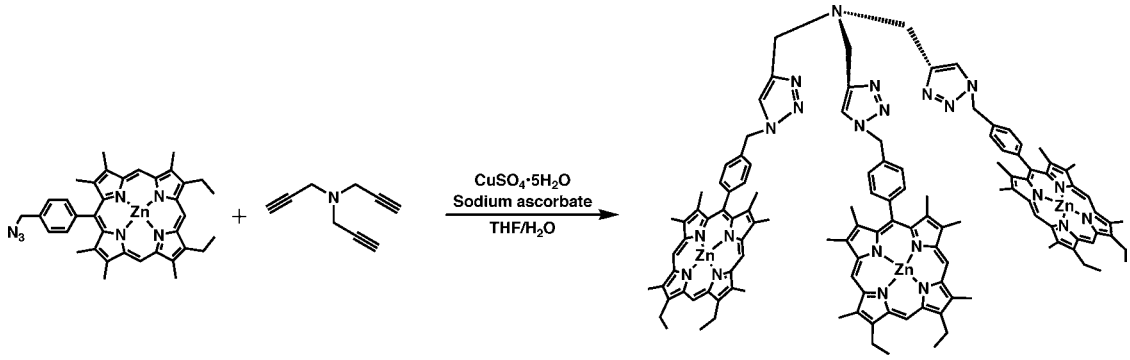


electron donor−acceptor system. The electron-transfer properties of the corresponding dimer $DPZn_2$ and monomer MPZn were also examined for comparison.

The electron-transfer properties of $TPZn_3$, $DPZn_2$, and MPZn were evaluated based on electrochemical (CV and DPV), vis−NIR, and ESR measurements. A supramolecular complex of $TPZn_3$ was formed with a fullerene derivative containing a pyridine moiety ($PyC_{60}$), which can be accommodated inside the cavity by $\pi-\pi$ interaction as well as by a coordination bond formed between $Zn^{2+}$ and the pyridine moiety. The photodynamics of the supramolecular complex ($TPZn_3-PyC_{60}$) was investigated by femtosecond and nanosecond laser flash photolysis measurements in nonpolar media. The present study provides the first example for investigations on $\pi$-bond formation in the oxidized multiporphyrins, which facilitates photoinduced electron transfer in a supramolecular complex of multiporphyrins with an electron acceptor in nonpolar media.[21a]

## Results and Discussion

**Synthesis and Physicochemical Characterization of Tripod Porphyrin $TPZn_3$.** We used click chemistry for the preparation of $TPZn_3$, because it is known to be a very selective and effective synthetic method, which can be performed under mild and clean conditions.[25] Many reports have already mentioned the utility of click chemistry of an azide and an ethynyl functionalized moiety for elaboration of sophisticated structures involving porphyrin as a backbone.[26] The synthetic procedure for the preparation of $TPZn_3$ is given in Scheme 2. The coupling reaction of 3 equiv of the azido zinc porphyrin and 1 equiv of commercially available tripropargylamine in the presence of $CuSO_4 \cdot 5H_2O$ and sodium ascorbate affords the tripod porphyrin.

The formation of $TPZn_3$ is clearly evidenced by the appearance on the MALDI/TOF mass spectrum of an ionic pattern at 2061.15 Da, which corresponds roughly to the radical cation species. Moreover, HR-MS measurements were performed using an ESI-QTOF technique on the isolated derivative, showing the presence of only two ions attributed to the mono- and disodium adducts. In both cases, the perfect match between experimental and simulated ionic patterns undoubtedly confirmed the structure of $TPZn_3$ (see Figure S1 in the Supporting Information for spectra). For example, the calculated mass for the monosodium adduct is equal to 2083.7838 Da, agreeing well with the experimental value found at 2083.7860 Da.

Characterization of the tripod porphyrin was also carried out using $^1$H NMR. At 500 MHz, the spectrum is well-resolved and quite easy to interpret if recorded at 328 K. A $C_3$ symmetry appears from the analysis of the spectrum, which leads to the equivalency of each of the three arms attached to the nitrogen atom. For example, the methylene protons close to the tertiary amine group appear as a broad singlet at 4.10 ppm. Conversely, the $CH_2$ protons located between the triazole motif and the phenyl group of the porphyrin ring are deshielded to be observed at 5.88 ppm. The multiplicities of the porphyrin proton signals are similar to those observed for the same protons for the starting azido porphyrin. However, all signals are slightly shielded compared to the corresponding ones for the azido derivative by approximately 0.5 ppm (see Experimental Section). This could account for some interaction between the porphyrin rings in the tripod under these solution conditions. The $^1$H NMR spectrum is given in the Supporting Information (Figure S2). MPZn[27] and $DPZn_2$ were also synthesized for comparison purposes. Physicochemical data for $DPZn_2$ are given in the Experimental Section.

(25) Kolb, H. C.; Finn, M. G.; Sharpless, K. B. *Angew. Chem., Int. Ed.* **2001**, *40*, 2004.

(26) (a) Trabolsi, A.; Elhabiri, M.; Urbani, M.; Delgado de la Cruz, J. L.; Ajamaa, F.; Solladié, N.; Albrecht-Gary, A.-M.; Nierengarten, J.-F. *Chem. Commun.* **2005**, 5736. (b) Meudtner, R. M.; Ostermeier, M.; Goddard, R.; Limberg, C.; Hecht, S. *Chem.—Eur. J.* **2007**, *13*, 9834. (c) Severac, M.; Le Pleux, L.; Scarpaci, A.; Blart, E.; Odobel, F. *Tetrahedron Lett.* **2007**, *48*, 6518. (d) Elmer, S. L.; Man, S.; Zimmerman, S. C. *Eur. J. Org. Chem.* **2008**, 3845. (e) Fazio, M. A.; Lee, O. P.; Schuster, D. I. *Org. Lett.* **2008**, *10*, 4979. (f) Liu, Y.; Ke, C.-F.; Zhang, H.-Y.; Cui, J.; Ding, F. *J. Am. Chem. Soc.* **2008**, *130*, 600. (g) Marois, J.-S.; Cantin, K.; Desmarais, A.; Morin, J.-F. *Org. Lett.* **2008**, *10*, 33. (h) Punidha, S.; Sinha, J.; Kumar, A.; Ravikanth, M. *J. Org. Chem.* **2008**, *73*, 323. (i) Santos, F. d. C.; Cunha, A. C.; de Souza, M. C. B. V.; Tome, A. C.; Neves, M. G. P. M. S.; Ferreira, V. F.; Cavaleiro, J. A. S. *Tetrahedron Lett.* **2008**, *49*, 7268. (j) Webb, J. E. A.; Maharaj, F.; Blake, I. M.; Crossley, M. J. *Synlett* **2008**, 2147. (k) Bakleh, M. E.; Sol, V.; Estieu-Gionnet, K.; Granet, R.; Deleris, G.; Krausz, P. *Tetrahedron* **2009**, *65*, 7385. (l) Collin, J.-P.; Frey, J.; Heitz, V.; Sauvage, J.-P.; Tock, C.; Allouche, L. *J. Am. Chem. Soc.* **2009**, *131*, 5609. (m) Fathalla, M.; Li, S.-C.; Diebold, U.; Alb, A.; Jayawickramarajah, J. *Chem. Commun.* **2009**, 4209. (n) Fiset, E.; Morin, J.-F. *Polymer* **2009**, *50*, 1369. (o) Hao, E.; Jensen, T. J.; Vicente, M. G. H. *J. Porphyrins Phthalocyanines* **2009**, *13*, 51. (p) Harriman, A.; Elliott, K. J.; Alamiry, M. A. H.; Le Pleux, L.; Severac, M.; Pellegrin, Y.; Blart, E.; Fosse, C.; Cannizzo, C.; Mayer, C. R.; Odobel, F. *J. Phys. Chem. C* **2009**, *113*, 5834. (q) Iehl, J.; Osinska, I.; Louis, R.; Holler, M.; Nierengarten, J.-F. *Tetrahedron Lett.* **2009**, *50*, 2245. (r) Ikawa, Y.; Harada, H.; Toganoh, M.; Furuta, H. *Bioorg. Med. Chem. Lett.* **2009**, *19*, 2448. (s) Jain, S. L.; Joseph, J. K.; Kuehn, F. E.; Reiser, O. *Adv. Synth. Catal.* **2009**, *351*, 230. (t) Liu, H.; Duclairoir, F.; Fleury, B.; Dubois, L.; Chenavier, Y.; Marchon, J.-C. *Dalton Trans.* **2009**, 3793. (u) McDonald, A. R.; Franssen, N.; van Klink, G. P. M.; van Koten, G. *J. Organomet. Chem.* **2009**, *694*, 2153. (v) Megiatto, J. D., Jr.; Spencer, R.; Schuster, D. I. *Org. Lett.* **2009**, *11*, 4152. (w) Palacin, T.; Khanh, H. L.; Jousselme, B.; Jegou, P.; Filoramo, A.; Ehli, C.; Guldi, D. M.; Campidelli, S. *J. Am. Chem. Soc.* **2009**, *131*, 15394. (x) Ringot, C.; Sol, V.; Granet, R.; Krausz, P. *Mater. Lett.* **2009**, *63*, 1889.

(27) Bellows, D.; Aly, S. M.; Gros, C. P.; Ojaimi, M. E.; Barbe, J.-M.; Guilard, R.; Harvey, P. D. *Inorg. Chem.* **2009**, *48*, 7613.

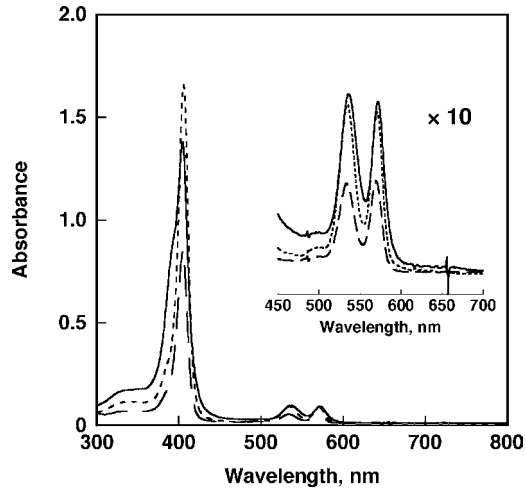


***Figure 1.*** UV−vis spectra of MPZn (— —), $DPZn_2$ (- - -), and $TPZn_3$ (—) at $3.0 \times 10^{-6}$ M in $CH_2Cl_2$ at 298 K.

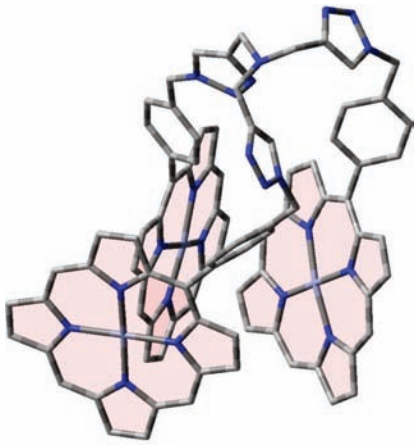

***Figure 2.*** Optimized structure of $TPZn_3$ calculated by DFT at the BLYP/3-21G(*) level. $\beta$-Substituents of $TPZn_3$ are replaced by protons for simplicity.

**Intramolecular $\pi-\pi$ Interaction between Porphyrin Rings of the Oxidized Tripod Porphyrins.** The intramolecular $\pi-\pi$ interaction between porphyrin moieties of the oxidized $TPZn_3$ was investigated by means of electrochemical (CV and DPV), UV−vis−NIR, ESR measurements, together with computational studies.

Figure 1 shows the UV−vis spectra of $TPZn_3$, $DPZn_2$, and MPZn. Both the Soret and Q bands of $TPZn_3$ are slightly shifted as compared to those of MPZn. Particularly, $TPZn_3$ exhibits a shoulder of Soret band at around 390 nm, which indicates the $\pi$-electron overlap between porphyrins in face-to-face conformation.[28]

The optimized structure of $TPZn_3$ is shown in Figure 2 (see Experimental Section for the calculation method). Each porphyrin in $TPZn_3$ is close to each other. Especially, two of three porphyrins in $TPZn_3$ have a face-to-face conformation. This optimized structure reflects the $\pi-\pi$ interaction as expected from the UV−vis spectrum of $TPZn_3$.

Electrochemical studies were performed by using cyclic voltammetry (CV) and differential pulse voltammetry (DPV) to investigate possible electronic interactions between porphyrin moieties in the oxidized states. Figure 3 shows the cyclic

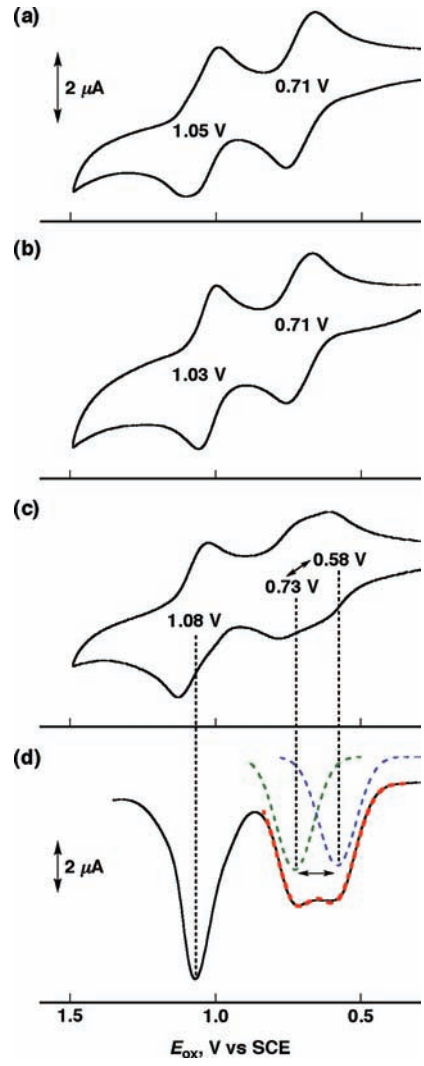


***Figure 3.*** Cyclic voltammograms (50 mV $s^{-1}$) of (a) MPZn, (b) $DPZn_2$, and (c) $TPZn_3$ in $CH_2Cl_2$ ($5 \times 10^{-4}$ M) containing 0.1 M $TBAPF_6$. (d) Differential pulse voltammograms of $TPZn_3$ under the same conditions as CV. The red line is the simulation curve using two discrete Gaussian-shape oxidation waves (blue and green lines).

voltammograms and differential pulse voltammograms of MPZn, $DPZn_2$, and $TPZn_3$ in $CH_2Cl_2$, respectively. MPZn exhibits two reversible redox waves which are typical for the sequential oxidation processes for zinc porphyrin: $MPZn/MPZn^{\bullet+}$ and $MPZn^{\bullet+}/MPZn^{2+}$. Similar redox waves are observed in the case of $DPZn_2$. Such redox behaviors indicate that each porphyrin in $DPZn_2$ behaves as a monomer porphyrin because it is geometrically independent, when the initial oxidation of two porphyrin moieties occurs at the same potential.

In contrast to the independent oxidation of two porphyrin moieties in $DPZn_2$ at the same potential, the initial three-electron oxidation of $TPZn_3$ is split into different steps. Because the sequential redox waves are close to each other, discrete redox waves are not observed even at a slow scan rate (10 mV $s^{-1}$). The initial oxidation wave obtained from DPV measurements can be simulated by multi Gaussian-shape oxidation waves, which ranged from 0.58 to 0.73 V. The next three-electron oxidation of $TPZn_3$ took place at the same potential (1.08 V).

All electrochemical data for MPZn, $DPZn_2$ and $TPZn_3$ are summarized in Table 1. The first oxidation potential of $TPZn_3$ (0.58 V in $CH_2Cl_2$) is lower than that of MPZn (0.71 V). This

(28) Satake, A.; Kobuke, Y. *Org. Biomol. Chem.* **2007**, *5*, 1679.

***Table 1.*** Oxidation Potentials of Porphyrins in $CH_2Cl_2$ and PhCN

| | $E_{ox}$, V vs SCE[a] | | |
|---|---|---|---|
| | MPZn | $DPZn_2$ | $TPZn_3$ |
| $CH_2Cl_2$ | 0.71 | 0.71 | 0.58−0.73 |
| | 1.05 | 1.03 | 1.08 |
| PhCN | 0.52 | 0.52 | 0.49 |
| | 0.88 | 0.87 | 0.90 |

[a] Measured in $CH_2Cl_2$ and PhCN containing 0.1 M $TBAPF_6$ at 298 K. The oxidation potentials of ferrocene as external standard are 0.52 and 0.34 V in $CH_2Cl_2$ and PhCN, respectively.

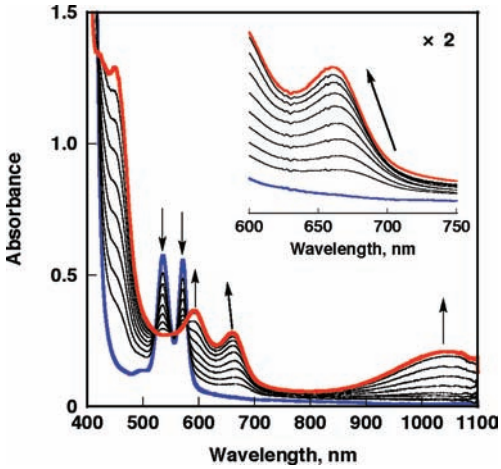


***Figure 4.*** vis−NIR spectral changes upon addition of $[Ru(bpy)_3]^{3+}$ (up to 3 equiv) to a $CH_2Cl_2$ solution of $TPZn_3$ ($1.7 \times 10^{-5}$ M) at 298 K.

is because the radical cation of trimer porphyrins is stabilized as compared to $MPZn^{\bullet+}$ due to the $\pi-\pi$ interaction between two porphyrin rings. Meanwhile, the rest of the oxidation potentials of $TPZn_3$ are higher than those of MPZn because of the electrostatic repulsion between porphyrin cations. The oxidation potentials in PhCN are also given in Table 1. It should be noted that no splitting of the initial redox waves of the trimer porphyrins was observed in PhCN (Figure S3), since PhCN can coordinate to zinc porphyrin to preclude any electronic communication between porphyrin rings.

The vis−NIR spectral titration of the trimer porphyrin was examined by using a one-electron oxidant, $[Ru(bpy)_3]^{3+}$. Upon addition of $[Ru(bpy)_3]^{3+}$ in MeCN to a $CH_2Cl_2$ solution of $TPZn_3$ at 298 K, new absorption bands at around 590 nm, 670 nm, and 1030 nm appear, and the absorption maximum at 670 nm is shifted to 660 nm, as shown in Figure 4. The absorption band at around 660 nm is typically assigned to the monomeric porphyrin radical cation (Figure S4).[29] This indicates that at the initial stage of electron-transfer oxidation of $TPZn_3$, the one-electron oxidized porphyrin interacts with the other neutral porphyrins,[30] which is consistent with the negative shift of the first oxidation potential of $TPZn_3$ as compared to that of MPZn. The appearance of NIR absorption bands ($\lambda_{max}$ = 1030 nm),

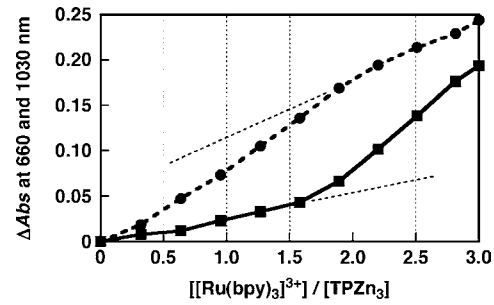


***Figure 5.*** Plots of absorption changes at 660 nm (dashed line with circle) and 1030 nm (solid line with square) vs concentration of oxidized $TPZn_3$ ($1.7 \times 10^{-5}$ M) in $CH_2Cl_2$ at 298 K.

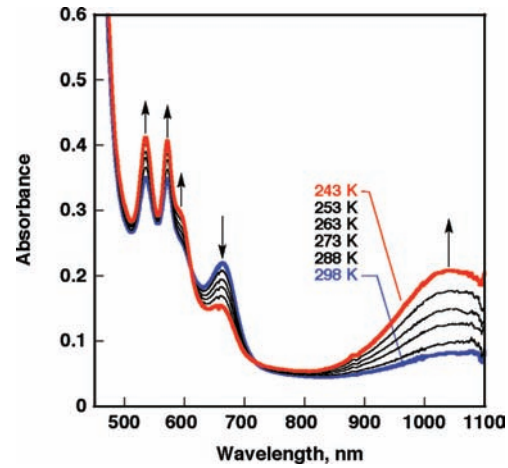


***Figure 6.*** vis−NIR spectral changes of a $CH_2Cl_2$ solution of $TPZn_3$ ($1.4 \times 10^{-5}$ M) in the presence of 2 equiv of $[Ru(bpy)_3]^{3+}$ at different temperatures.

the so-called charge-resonance band, indicates the existence of electronic interaction between porphyrin radical cations.[31,32]

In sharp contrast to what is observed for $TPZn_3$, there is no change in the NIR region when MPZn and $DPZn_2$ are oxidized by $[Ru(bpy)_3]^{3+}$ under the same conditions (Figures S4).[33] Figure 5 shows the absorbance changes at 660 and 1030 nm. The absorbance at 1030 nm slightly increases until the addition of ca. 1.5 equiv of $[Ru(bpy)_3]^{3+}$, followed by a large increase to give the largest value at $[[Ru(bpy)_3]^{3+}]/[TPZn_3^{3+}] = 3$, where all of the porphyrins are one-electron oxidized. Thus, the NIR band is attributed to the electronic interaction among porphyrin radical cations. In such a case, there are two possibilities to show the charge resonance band: the charge delocalization (i) among three porphyrin rings and (ii) between two of three porphyrin rings. In order to clarify this point, the vis−NIR and ESR spectra of $TPZn_3^{2+}$ were measured under the same conditions. Figures 6 and 7 depict the temperature dependence of vis−NIR and ESR spectra, respectively. As the temperature of a $CH_2Cl_2$ solution of $TPZn_3^{2+}$ decreases, the absorbance at 660 nm derived from the monomeric porphyrin radical cation decreases, while the charge resonance band ($\lambda_{max}$ = 1030 nm) and Q bands of neutral $TPZn_3$ increase (Figure 6).

(29) (a) Fajer, J.; Borg, D. C.; Forman, A.; Dolphin, D.; Felton, R. H. *J. Am. Chem. Soc.* **1970**, *92*, 3451. (b) Fuhrhop, J. H.; Wasser, P.; Riesner, D.; Mauzerall, D. *J. Am. Chem. Soc.* **1972**, *94*, 7996.

(30) The characteristic NIR absorption ($\lambda_{max} \approx 3000$ nm) due to the interaction between neutral porphyrin and radical cation was not clearly observed by vis−NIR spectroscopy, because electron-transfer oxidation states of $TPZn_3$ are in equilibria to afford stable $TPZn_3^{2+}$ prior to $TPZn_3^{\bullet+}$, and the absorption coefficient of $TPZn_3^{\bullet+}$ in NIR region may be too small (see ref 24).

(31) Kochi, J. K.; Rathore, R.; Magueres, P. L. *J. Org. Chem.* **2000**, *65*, 6826.

(32) Both of the NIR absorption and visible absorption due to the monomeric porphyrin radical cation disappear when more than 3 equiv of a MeCN solution of $[Ru(bpy)_3]^{3+}$ is added (see Figure S5 in the Supporting Information).

(33) The ratio of absorbance at 660 and 1030 nm of $TPZn_3$ is the same irrespective of the concentration. These results indicate that the NIR band of $TPZn_3^{n+}$ ($0 < n \leq 3$) is due to intramolecular interaction.

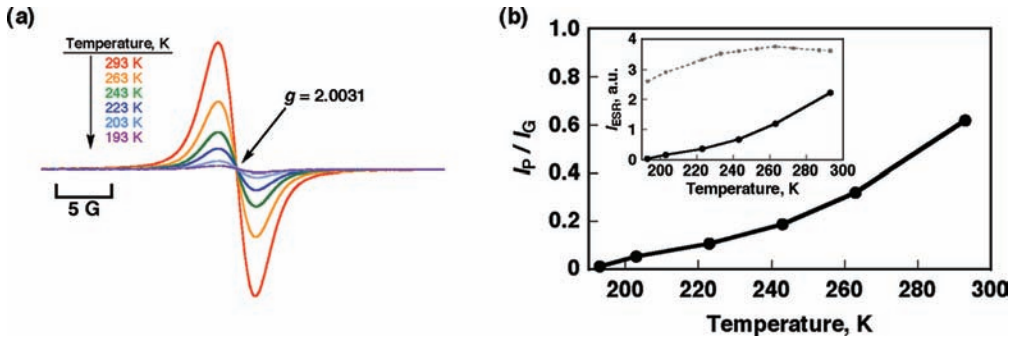


***Figure 7.*** (a) ESR spectral changes of a $CH_2Cl_2$ solution of $TPZn_3$ ($1.6 \times 10^{-4}$ M) in the presence of 2 equiv of $[Ru(bpy)_3]^{3+}$ at different temperatures. (b) Dependence of the ratio of the ESR intensity ($I_P/I_G$, where $I_P$ and $I_G$ is the ESR intensity of $TPZn_3^{2+}$ and galvinoxyl radical, respectively) on the temperature. The ESR intensity was determined by double integration of the corresponding first-derivative ESR spectrum. Inset: Dependence of the ESR intensity ($I_P$, solid line and $I_G$, dashed line) on the temperature. Both of the concentrations of $TPZn_3^{2+}$ and galvinoxyl radical are $1.6 \times 10^{-4}$ M and $3.2 \times 10^{-4}$ M in $CH_2Cl_2$, respectively.

***Scheme 3***

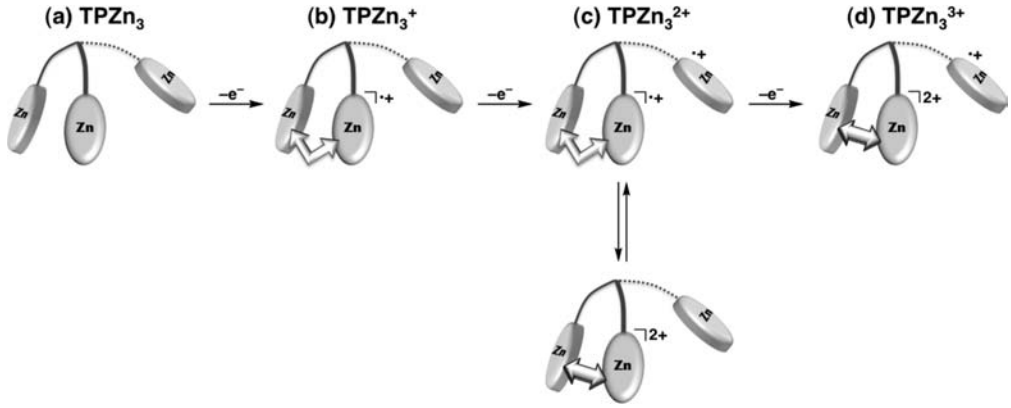


This suggests that at low temperature, the charge of $TPZn_3^{2+}$ is delocalized between two porphyrins only to form a dimeric radical cation, and the other porphyrin behaves like a neutral monomer porphyrin. In addition, the ESR intensity of $TPZn_3^{2+}$ changes reversibly and decreases precipitously when lowering the temperature, as shown in Figure 7. The quantitative analysis of the ESR intensity was performed to distinguish the inherent radical concentrations of $TPZn_3^{2+}$ from the Curie law and instrumental factors (see Experimental Section for details). The $I_P/I_G$ value at 293 K (0.62) indicates that 38% of the oxidized porphyrins form diamagnetic species in $TPZn_3^{2+}$, which is fairly consistent with the vis−NIR measurements as shown in Figures 4 and 5.[34] If the charge of $TPZn_3^{2+}$ were delocalized among three porphyrin rings, the minimum ESR intensity should be one-third of the initial ESR intensity. Therefore, the major drop in signal intensity can be assigned to the formation of diamagnetic ESR-silent species, according to the spin coupling between two porphyrin radical cations (for molecular orbital diagrams, see Figure S7b).[35] Such a temperature dependence of vis−NIR and ESR spectra also indicates the existence of an equilibrium between two electronic states of $TPZn_3^{2+}$ as described later. The strong interaction between two of the three porphyrins is consistent with the optimized structure obtained by DFT calculation (Figure 2).

By combining the above results with the electrochemical data obtained by CV and DPV, the electron-transfer oxidation process of $TPZn_3$ can be summarized as illustrated in Scheme 3. First, the one-electron oxidized porphyrin interacts with the adjacent porphyrin to form a $\pi$-bond, which stabilizes the dimer radical cation as compared to monomer porphyrin radical cation (Figure S7a). The negative shift of the first oxidation potential of $TPZn_3$ proves the existence of such an interaction, together with the shift of the absorption maximum from 670 to 660 nm. The two-electron oxidized state, $TPZn_3^{2+}$, exists in equilibrium between the following two states: (i) one electron is delocalized between two adjacent porphyrins and the other electron is localized on the porphyrin which is sterically independent, and (ii) two electrons are delocalized between two adjacent porphyrins. The latter is more favorable at lower temperature, contrary to the case of *meso*−*meso* linked porphyrin dimer reported in the literature.[36,37] Finally, in the three-electron oxidized state, all of the porphyrins of $TPZn_3$ are one-electron oxidized to afford monomeric and dimeric porphyrin radical cations (Scheme 3c). To the best of our knowledge, this is the first example to show the stepwise electron-transfer oxidation and $\pi$-bond formation of tripod porphyrin system.

**Complex Formation of Tripod Porphyrin with *p*-Pyridyl Fulleropyrrolidine.** The electrochemical (CV and DPV), vis−NIR, and ESR spectroscopic studies depicted the interchromophoric interactions of $TPZn_3$ through $\pi-\pi$ interactions, particularly in

(34) Comparison of the ESR intensities of $[TPZn_3]^{n+}$ ($0 < n \leq 3$) is shown in Figure S6 (in the Supporting Information). The ESR intensities of $TPZn_3^{2+/3+}$ are quite smaller relative to the values expected from the linear increase of ESR intensity of $TPZn_3^{\bullet+}$, which is again consistent with the vis−NIR measurements as shown in Figures 4 and 5.

(35) Lü, J.-M.; Rosokha, S. V.; Kochi, J. K. *J. Am. Chem. Soc.* **2003**, *125*, 12161.

(36) Segawa, H.; Senshu, Y.; Nakazaki, J.; Susumu, K. *J. Am. Chem. Soc.* **2004**, *126*, 1354.

(37) In any oxidized states of $TPZn_3^{n+}$ ($0 < n \leq 3$), no triplet signal was observed by ESR spectroscopy at 77 K.

the one, two, and three electron-oxidized states. The flexible tripod linker allows such electronic interactions. Additionally, the geometric feature of $TPZn_3$ makes it possible to capture of guest molecules inside the cavity of the tripod efficiently through noncovalent interactions and coordination bond.[20f,38,39] Here, we demonstrate the complexation behavior of $TPZn_3$ with *N*-methyl-2-(*p*-pyridyl)fulleropyrrolidine ($PyC_{60}$) in comparison with MPZn and $DPZn_2$ (Scheme 4). Fullerene derivatives

***Scheme 4***

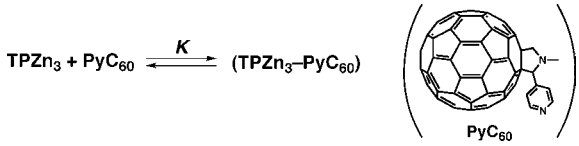


generally exhibit noteworthy electron acceptor properties in combination with appropriate $\pi$-conjugated electron donors,[40] and $PyC_{60}$ is known to bind with monomer zinc porphyrin by axial coordination in nonpolar media such as toluene and *o*-dichlorobenzene.[8a]

UV−vis spectral changes were recorded during the complexation of $TPZn_3$ with $PyC_{60}$ in *o*-dichlorobenzene as shown in Figure 8. The original Soret band of $TPZn_3$ ($\lambda_{max} = 410$ nm) decreases in intensity and all the visible bands due to $TPZn_3$ are red-shifted. The red shift of the Soret band is widely known for the formation of the coordination bond.[8a] The absorbance change of the Soret band at 410 nm is shown in Figure 9a. Once the absorption decreases, the absorption increases linearly due to the absorption of $PyC_{60}$. The inset in Figure 9a exhibits the Soret band spectral change subtracted from the absorption of $PyC_{60}$. Job's plot of continuous variation method was run to confirm the stoichiometry of the complex (Figure S9). The plot exhibits a broad curve with a maximum value, 0.46. This result indicates that a 1:1 complex (theoretical maximum is 0.50) is formed as a major product.[41] The association constant $K$ of $TPZn_3$−$PyC_{60}$ (1:1) complex is determined from the $\Delta$Abs at 410 nm.[42] From a linear plot of $[TPZn_3]/(\Delta A_0 - \Delta A)$ versus $[PyC_{60}]^{-1}$ at 410 nm (Figure 9b), where $\Delta A_0$ and $\Delta A$ are the

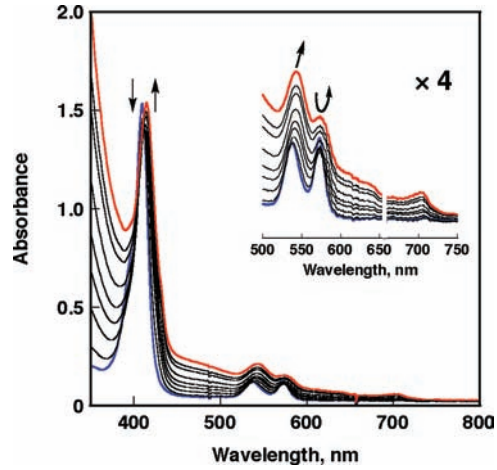


***Figure 8.*** UV−vis spectral changes upon addition of $PyC_{60}$ (0 to $4.8 \times 10^{-5}$ M) to an *o*-dichlorobenzene solution of $TPZn_3$ ($3.0 \times 10^{-6}$ M) at 298 K.

$\Delta$Abs at 410 nm in the absence and presence of $PyC_{60}$, the association constant $K$ is determined to be $9.4 \times 10^4$ $M^{-1}$ in *o*-dichlorobenzene at 298 K.

As $TPZn_3$ forms the supramolecular complex with $PyC_{60}$, the fluorescence emission of $TPZn_3$ is quenched by intracomplex electron transfer from the singlet excited state of $TPZn_3$ moiety to $PyC_{60}$ in nonpolar media (Figure S10a). The association constant $K$ of $TPZn_3$−$PyC_{60}$ complex is also obtained as $5.5 \times 10^4$ $M^{-1}$ from the change in the fluorescence intensity at 577 nm (Figure S10b). The $K$ value estimated from the fluorescence quenching is slightly smaller than that determined from the UV−vis spectral change, because the intermolecular dynamic quenching process between $TPZn_3$ moiety and free $PyC_{60}$ is not negligible at relatively high concentrations of $PyC_{60}$, and the absorption of $TPZn_3$ at the excitation wavelength is overlapped with that of $PyC_{60}$ to decrease the original fluorescence emission of $TPZn_3$.

UV−vis measurements were similarly examined for MPZn and $DPZn_2$ to determine the association constants $K$ with $PyC_{60}$. The $K$ value of $DPZn_2$ in each solvent (toluene and *o*-dichlorobenzene) is much smaller as compared with that of $TPZn_3$. In the case of MPZn, UV−vis spectral change during the complexation with $PyC_{60}$ is too small to determine the $K$ value accurately. Thus, the association constants were determined by means of $^1$H NMR titration. Figures 10 and S11 depict the spectral changes of $TPZn_3$ and MPZn, respectively, upon addition of $PyC_{60}$ to a $CDCl_3/CS_2$ (1:1 *v*/*v*) mixture at room temperature. The $^1$H NMR signals of $TPZn_3$ exhibit downfield shifts upon complexation with $PyC_{60}$ as shown in Figure 10. Meanwhile, the pyridyl protons of $PyC_{60}$ exhibit large upfield shifts by the complexation, which is ascribed to the influence of the large porphyrin aromatic ring current. This result clearly shows that the pyridyl group of $PyC_{60}$ coordinates to the central zinc ions of $TPZn_3$. The signal of the free $TPZn_3$ and the complexed $TPZn_3$ always coalesce into a single signal. This indicates that the complexation and exchange between different zinc ions takes place faster than the NMR time scale. The association constant of $TPZn_3$−$PyC_{60}$ complex is determined from the peak shift of the *meso*-proton signals of $TPZn_3$ using eq 1[43]

$$\delta_{obs} = \delta_H + (\delta_{HG} - \delta_H) \times \frac{([H_t] + [G_t] + 1/K) - \{([H_t] + [G_t] + 1/K)^2 - 4[H_t][G_t]\}^{1/2}}{2[H_t]} \quad (1)$$

(38) Tong, L. H.; Pascu, S. I.; Jarrosson, T.; Sanders, J. K. *Chem. Commun.* **2006**, 1085.

(39) The complex behavior between $TPZn_3$ and pristine $C_{60}$ was investigated with $^1$H NMR spectroscopy. The protons of $TPZn_3$ in $CDCl_3/CS_2$ (1:1 *v*/*v*) slightly changed upon addition of pristine $C_{60}$ as shown in Figure S8a−c, while that of MPZn exhibited little change (Figure S8d−f). It is difficult to determine the association constant between $TPZn_3$ and $C_{60}$ because of its small value and limited solubility. Nevertheless, the $^1$H NMR signals of *meso*-protons of $TPZn_3$ (9.52 and 9.46 ppm) tended to be simplified into a single signal by the addition of $C_{60}$, as was observed for the complexation between $TPZn_3$ and $PyC_{60}$. Thus, pristine $C_{60}$ is also incorporated inside the cavity of $TPZn_3$. These results indicate that $\pi-\pi$ interactions between $TPZn_3$ and fullerene $\pi$-sphere strongly assist the coordination bond between the zinc ion of $TPZn_3$ and the pyridyl group of $PyC_{60}$.

(40) (a) Guldi, D. M.; Rahman, G. M. A.; Marczak, R.; Matsuo, Y.; Yamanaka, M.; Nakamura, E. *J. Am. Chem. Soc.* **2006**, *128*, 9420. (b) Marczak, R.; Wielopolski, M.; Gayathri, S. S.; Guldi, D. M.; Matsuo, Y.; Matsuo, K.; Tahara, K.; Nakamura, E. *J. Am. Chem. Soc.* **2008**, *130*, 16207. (c) Matsuo, Y.; Maruyama, M.; Gayathri, S. S.; Uchida, T.; Guldi, D. M.; Kishida, H.; Nakamura, A.; Nakamura, E. *J. Am. Chem. Soc.* **2009**, *131*, 12643. (d) Sandanayaka, A. S. D.; Ito, O.; Tanaka, T.; Isobe, H.; Nakamura, E.; Yudasaka, M.; Iijima, S. *New J. Chem.* **2009**, *33*, 2261. (e) Guldi, D. M.; Illescas, B. M.; Atienza, C. M.; Wielopolskia, M.; Martin, N. *Chem. Soc. Rev.* **2009**, *38*, 1587, and references therein.

(41) A 1:2 complex (theoretical maximum is 0.33) may be also formed as a minor species.

(42) Fukuzumi, S.; Kondo, Y.; Mochizuki, S.; Tanaka, T. *J. Chem. Soc., Perkin Trans. 2* **1989**, 1753.

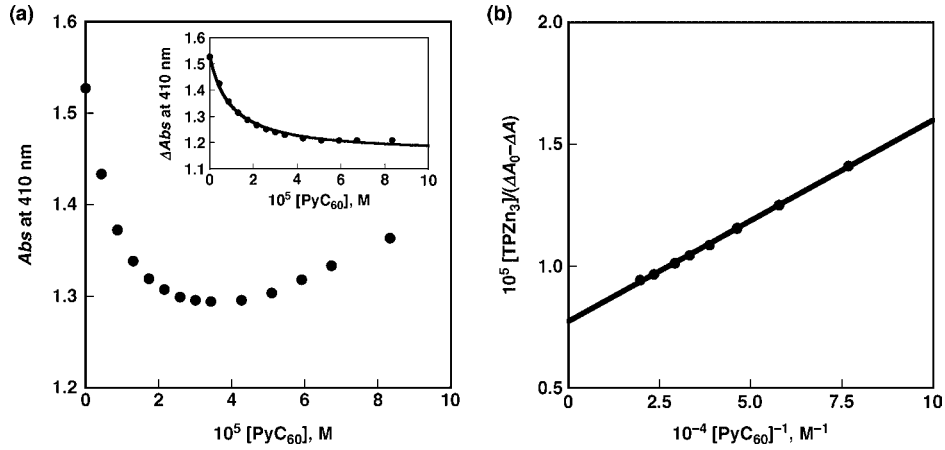


***Figure 9.*** (a) Original spectral change at 410 nm due to $TPZn_3$ with increasing concentration of $PyC_{60}$ in *o*-dichlorobenzene at 298 K. Inset: ΔAbs at 410 nm. (b) Plot of $[TPZn_3]_0/(A_0 - A)$ vs $[PyC_{60}]^{-1}$.

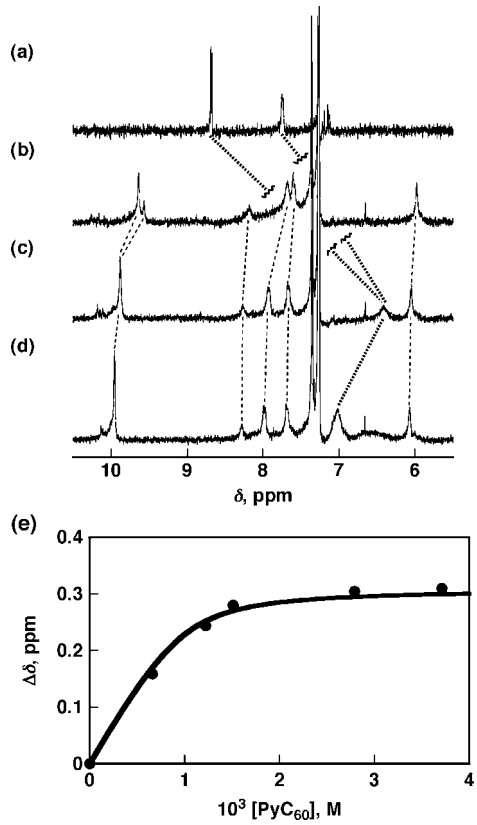


***Figure 10.*** $^1H$ NMR spectra of (a) $PyC_{60}$, (b) $TPZn_3$ ($1.0 \times 10^{-3}$ M), and (c and d) $TPZn_3$ ($1.0 \times 10^{-3}$ M) in the presence of $PyC_{60}$; (c) $1.2 \times 10^{-3}$ M and (d) $3.7 \times 10^{-3}$ M in $CDCl_3/CS_2$ (1:1 *v*/*v*). The dashed lines represents the spectral changes due to $TPZn_3$, whereas the dotted lines represents the spectral changes due to pyridine moieties of $PyC_{60}$. (e) Change in the chemical shift of the *meso*-protons of $TPZn_3$ upon addition of $PyC_{60}$. The curve represents the best fit according to eq 1.

where $[H_t]$ and $[G_t]$ are total host and guest concentrations, respectively, $\delta_{obs}$ is the observed shift, $\delta_H$ is the chemical shift of the host, $\delta_{HG}$ is the chemical shift of the host−guest complex, and *K* is the association constant. From a fitting curve shown in Figure 10e, the *K* value of $TPZn_3$ is determined to be $1.1 \times 10^4$ $M^{-1}$ in $CDCl_3/CS_2$ (1:1 *v*/*v*) at 298 K. Likewise, the *K* values of $DPZn_2$ and MPZn were evaluated from $^1H$ NMR titration (see Figure S11 for MPZn) and the results are given in Table 2. It should be noted that the signals of MPZn and $DPZn_2$ exhibit upfield shifts during the complexation, whereas the signals of $TPZn_3$ exhibit downfield shifts as mentioned above. If $PyC_{60}$ bound to $TPZn_3$ only by axial coordination, the signals of $TPZn_3$ should shift in a similar way to those of MPZn. Thus, $PyC_{60}$ is captured inside the cavity of $TPZn_3$ not only by a coordination bond but also $\pi-\pi$ interactions, which cause the downfield shifts of protons in $TPZn_3$.[20f,22a,43]

***Table 2.*** Association Constants (*K*, $M^{-1}$) of Porphyrins with $PyC_{60}$

| | *K*, $M^{-1}$ | | |
|---|---|---|---|
| | MPZn | $DPZn_2$ | $TPZn_3$ |
| $CDCl_3/CS_2$ (1:1 *v*/*v*) | $9.4 \times 10^2$ | $2.3 \times 10^3$ | $1.1 \times 10^4$ |
| *o*-dichlorobenzene | [a] | $5.9 \times 10^3$ | $9.4 \times 10^4$ |
| toluene | [a] | $3.9 \times 10^4$ | $1.1 \times 10^5$ |

[a] Little UV−vis spectral changes were observed to preclude the determination of the *K* values.

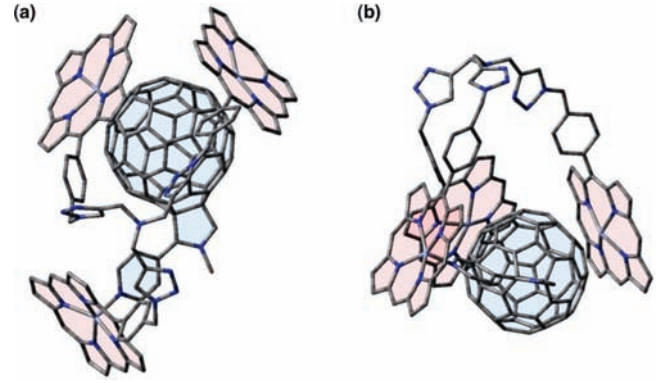


***Figure 11.*** Optimized structure of $TPZn_3-PyC_{60}$ complex calculated by DFT at the BLYP/3-21G(*) level: (a) top view and (b) side view. β-Substituents of $TPZn_3$ are replaced by protons for simplicity.

The *K* values increase in the order MPZn < $DPZn_2$ < $TPZn_3$. The enhanced binding ability of $TPZn_3$ again results from $\pi-\pi$ interactions between $TPZn_3$ and $PyC_{60}$ which is embedded into the cavity of $TPZn_3$.

The DFT calculation (B3LYP/3-21G(*) basis set) also supports the encapsulation of $PyC_{60}$ into the cavity of $TPZn_3$ (see Figure 11). The distance of axial coordination bond (Zn−N) is found to be 2.00 Å, which is quite similar to the values reported previously.[8a] The minimum distances between the other porphyrin planes and fullerene are found to be 2.58 and 2.63

(43) Miyazaki, S.; Ohkubo, K.; Kojima, T.; Fukuzumi, S. *Angew. Chem., Int. Ed.* **2007**, *46*, 905.

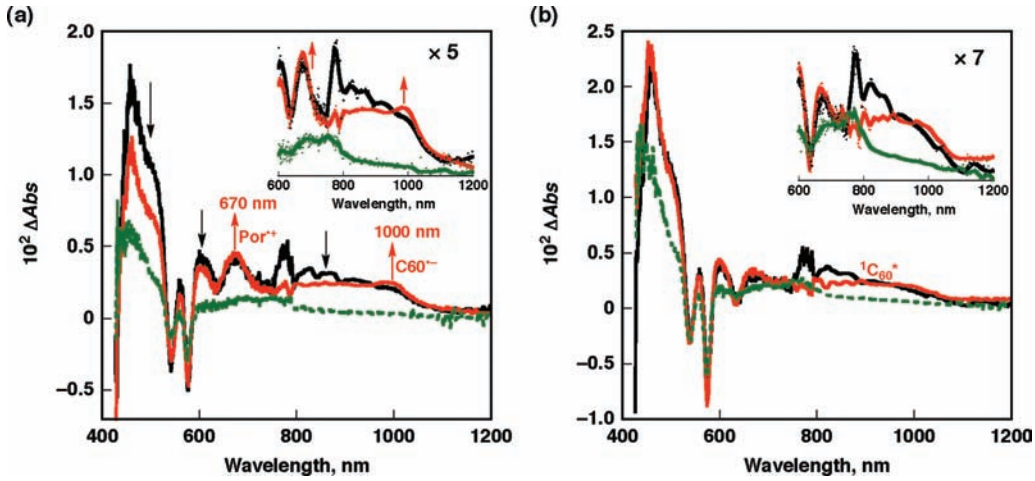


***Figure 12.*** Differential transient absorption spectra of (a) $TPZn_3$ ($7.0 \times 10^{-6}$ M) and (b) MPZn ($1.1 \times 10^{-5}$ M) in the presense of $PyC_{60}$ ($2.3 \times 10^{-5}$ M) obtained at 2 (black), 62 (red), and 2800 ps (green) after femtosecond laser pulse irradiation at 410 nm in deaerated toluene at 298 K.

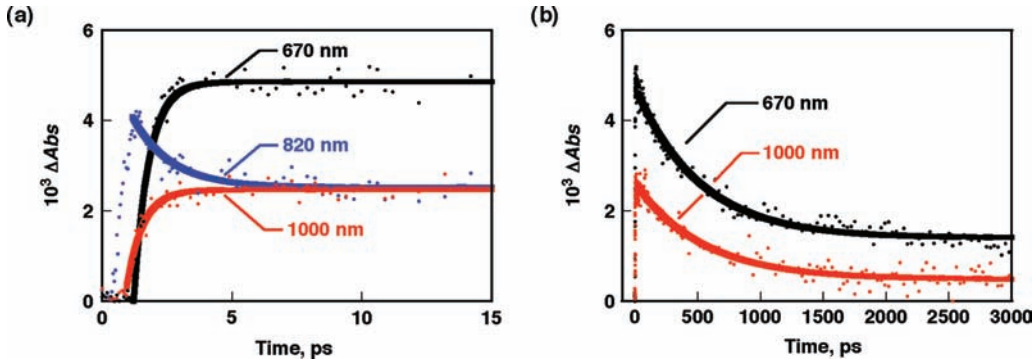


***Figure 13.*** (a) Time profiles of differential transient absorption spectra for $TPZn_3$ ($7.0 \times 10^{-6}$ M) in the presense of $PyC_{60}$ ($2.3 \times 10^{-5}$ M) at 0−15 ps time intervals. (b) Time profiles of differential transient absorption spectra for $TPZn_3$ in the presense of $PyC_{60}$ at 0−3000 ps time intervals. Each curve monitored at 670 (black), 820 (blue), and 1000 nm (red) represents the best fit to the first-order rise and decay.

Å, respectively. These values of spatial separation suggest possible $\pi-\pi$ interactions, which are consistent with the crystallographic studies of porphyrin-fullerene systems.[20f,44]

**Photoinduced Electron Transfer from Tripod Porphyrin to $PyC_{60}$.** Time-resolved transient absorption spectra of $TPZn_3$ and MPZn in the presence of $PyC_{60}$ were recorded by femtosecond laser flash photolysis in deaerated toluene, as shown in Figure 12. From UV−vis spectral changes, $TPZn_3$ mainly exists as a complex $TPZn_3-PyC_{60}$, whereas MPZn scarcely forms complex with $PyC_{60}$ because of its small association constant. The absorption spectrum observed 2 ps after the laser pulse (black line) exhibits absorption bands which are unambiguously assigned to the singlet excited states of the porphyrin moieties, $^1TPZn_3^*-PyC_{60}$ (Figure 12a) and $^1$MPZn* (Figure 12b), respectively.[45] The transient absorption spectrum due to $^1TPZn_3^*-PyC_{60}$ changes as time elapses to afford another absorption band at 62 ps after the laser pulse (red line). The absorption band observed at $\lambda_{max} = 1000$ nm is clearly attributed to the monofunctionalized fullerene radical anion.[8a,46] The accompanying absorption band at 670 nm corresponds to the absorption spectrum of one-electron oxidized species of $TPZn_3$ ($TPZn_3^{\bullet+}$) which is observed by vis−NIR spectroscopy (Figure 4).[8a,46d−g] The rise of the absorptions at 670 and 1000 nm affords an apparent first-order rate constant ($k_{ET}$) of $6.4 \times 10^{11}$ $s^{-1}$ (Figure 13a). In addition, the decay of the band at 820 nm due to $^1TPZn_3^*$ is related to the rise of the absorptions at 670 and 1000 nm. All these observations are in accordance with the intracomplex electron transfer from $^1TPZn_3^*$ to $PyC_{60}$ affording the radical ion pair state ($TPZn_3^{\bullet+}-PyC_{60}^{\bullet-}$). At 2800 ps, the absorption at 670 and 1000 nm decay with a first-order rate constant of $1.9 \times 10^9$ $s^{-1}$ (Figure 13b). We assigned this process to the intracomplex back electron transfer from $PyC_{60}^{\bullet-}$

(44) (a) Sun, D.; Tham, F. S.; Reed, C. A.; Chaker, L.; Boyd, P. D. *J. Am. Chem. Soc.* **2002**, *124*, 6604. (b) Olmstead, M. M.; Costa, D. A.; Maitra, K.; Noll, B. C.; Phillips, S. L.; Van Calcar, P. M.; Balch, A. L. *J. Am. Chem. Soc.* **1999**, *121*, 7090. (c) Boyd, P. D. W.; Hodgson, M. C.; Rickard, C. E. F.; Oliver, A. G.; Chaker, L.; Brothers, P. J.; Bolskar, R. D.; Tham, F. S.; Reed, C. A. *J. Am. Chem. Soc.* **1999**, *121*, 10487.

(45) Rodriguez, J.; Kirmaier, C.; Holten, D. *J. Am. Chem. Soc.* **1989**, *111*, 6500.

(46) (a) Guldi, D. M.; Prato, M. *Acc. Chem. Res.* **2000**, *33*, 695. (b) Fukuzumi, S.; Ohkubo, K.; Imahori, H.; Shao, J.; Ou, Z.; Zheng, G.; Chen, Y.; Pandey, R. K.; Fujitsuka, M.; Ito, O.; Kadish, K. M. *J. Am. Chem. Soc.* **2001**, *123*, 10676. (c) Ohkubo, K.; Kotani, H.; Shao, J.; Ou, Z.; Kadish, K. M.; Li, G.; Pandey, R. K.; Fujitsuka, M.; Ito, O.; Imahori, H.; Fukuzumi, S. *Angew. Chem., Int. Ed.* **2004**, *43*, 853. (d) Schuster, D. I.; Loa, K.; Guldi, D. M.; Palkar, A.; Echegoyen, L.; Stanisky, C.; Cross, R. J.; Niemi, M.; Tkachenko, N. V.; Lemmetyinen, H. *J. Am. Chem. Soc.* **2007**, *129*, 15973. (e) Imahori, H.; Tamaki, K.; Guldi, D. M.; Luo, C.; Fujitsuka, M.; Ito, O.; Sakata, Y.; Fukuzumi, S. *J. Am. Chem. Soc.* **2001**, *123*, 2607. (f) Imahori, H.; Guldi, D. M.; Tamaki, K.; Yoshida, Y.; Luo, C.; Sakata, Y.; Fukuzumi, S. *J. Am. Chem. Soc.* **2001**, *123*, 6617. (g) D'Souza, F.; Maligaspe, E.; Karr, P. A.; Schumacher, A. L.; Ojaimi, M. E.; Gros, C. P.; Barbe, J.-M.; Ohkubo, K.; Fukuzumi, S. *Chem.—Eur. J.* **2008**, *14*, 674.

***Table 3.*** Luminescence Data for MPZn, $DPZn_2$, and $TPZn_3$

| compound | $E(S_1)$, eV[a] | $\tau_{fl}$, ns[b] | $\Phi_{fl}$[b] | $E(T_1)$, eV[c] |
|---|---|---|---|---|
| MPZn | 2.16 | 2.24 ± 0.12 | 0.024 | 1.77 |
| $DPZn_2$ | 2.16 | 1.92 ± 0.06 | 0.022 | 1.76 |
| $TPZn_3$ | 2.16 | 2.10 ± 0.07 | 0.016 | 1.76 |

[a] Determined from the absorption and fluorescence spectra in toluene at 298 K. [b] Measured in toluene at 298 K. [c] Measured in 2-MeTHF at 77 K.

to $TPZn_3^{\bullet+}$ to recover the ground state of the complex $TPZn_3-PyC_{60}$. The slightly remained absorption spectrum (highlighted in green in Figure 12a) may be derived from the triplet excited states of uncomplexed free $TPZn_3$ and $PyC_{60}$.

In sharp contrast to the $TPZn_3-PyC_{60}$ complex system, the transient absorption spectrum of MPZn in the presence of $PyC_{60}$ (Figure 12b) exhibits no characteristic absorption at 670 nor 1000 nm assigned to $MPZn^{\bullet+}$ and $PyC_{60}^{\bullet-}$, respectively. The transient absorption spectrum obtained 62 ps after the laser pulse (red line in Figure 12b) exhibits the slight increase of the broad absorption in visible/NIR region and decrease of the absorption at around 800 nm. Such a spectral change from $^1$MPZn* (black line in Figure 12b) can be assigned to the energy transfer from MPZn to $PyC_{60}$ to give the singlet excited state $^1PyC_{60}$* (1.76 eV: determined from the absorption and fluorescence spectra).[46e] The $^1$MPZn* as well as $^1PyC_{60}$* result in the formation of the triplet excited states $^3$MPZn* and $^3PyC_{60}$* at 2800 ps (green line in Figure 12b), accompanied by the recovery of the ground state.

The singlet energy levels of porphyrins ($E(S_1)$) are listed in Table 3, together with the fluorescence lifetimes ($\tau_{fl}$), the fluorescence quantum yields ($\Phi_{fl}$), and the triplet energy levels ($E(T_1)$). The cyclic voltammograms of $TPZn_3$ in the absence and presence of $PyC_{60}$ in $CH_2Cl_2$/*o*-dichlorobenzene (1:1 *v*/*v*) are shown in Figure S12. Interestingly, in the presence of $PyC_{60}$, only the first oxidation process of $TPZn_3$ exhibits reversible redox waves, and the first oxidation of $TPZn_3$ moiety and first reduction of $PyC_{60}$ moiety are found at +0.63 and −0.61 V, respectively. The first oxidation potential (0.63 V) is similar to that of $TPZn_3$ in the absence of $PyC_{60}$ (0.61 V). This indicates that the one-electron oxidized state of the $TPZn_3-PyC_{60}$ complex ($TPZn_3^{\bullet+}-PyC_{60}$) is stabilized by electronic interaction between porphyrins even in the presence of $PyC_{60}$. Electrochemical measurement was similarly examined for MPZn in the presence of $PyC_{60}$, and reversible redox waves were observed at +0.73 and −0.61 V, respectively.

Based on the photophysical and electrochemical data of porphyrins as well as fullerene derivatives, the energy diagrams of photochemical events for $TPZn_3$ and MPZn in the presence of $PyC_{60}$ in toluene are summarized in Scheme 5, parts a and b, respectively. When the solvent is different from the one used in the electrochemical determinations, the electrochemical potentials are corrected by using the Born dielectric continuum model.[47,48] In the present case, $\varepsilon_s = 2.4$ is used as the dielectric constant of toluene. The $\varepsilon_p$ value is taken as 9.6, an average of the dielectric constant of $CH_2Cl_2$ (8.9) and of *o*-dichlorobenzene (10.4). Thus, the energy level of the charge-separated states ($TPZn_3^{\bullet+}$-$PyC_{60}^{\bullet-}$) is calculated as 1.49 eV in toluene, which is lower than the energy level of the triplet excited state of $PyC_{60}$ moieties (1.56 eV).[49] The $k_{ET}$ value is sufficiently large relative to the rate constant of intersystem crossing, which enables the photoinduced electron transfer from $TPZn_3$ to $PyC_{60}$. From the rate constant of back electron transfer ($k_{BET} = 1.9 \times 10^9$ s$^{-1}$), the lifetime of the charge-separated state ($TPZn_3^{\bullet+}-PyC_{60}^{\bullet-}$) is determined to be $\tau_{CS} = 0.53$ ns. On the other hand, only energy transfer from $^1$MPZn* to $PyC_{60}$ takes place to produce $^1PyC_{60}$*, in competition with intersystem crossing to $^3$MPZn*, following the formation of $^3PyC_{60}$*. The intermolecular electron transfer from MPZn to $PyC_{60}$ was not observed in nanosecond laser flash photolysis measurements.

$TPZn_3$ can bind $PyC_{60}$ much stronger than MPZn or $DPZn_2$, which allows a strong electron donor−acceptor complex to form. The intracomplex electron transfer from $^1TPZn_3$* to $PyC_{60}$ occurs, whereas no electron transfer from $^1$MPZn* to $PyC_{60}$ occurs under the same experimental conditions due to the weak binding of $PyC_{60}$ to MPZn. Such enhanced electron-transfer properties of $TPZn_3$ relative to MPZn and $DPZn_2$ may be derived from the $\pi-\pi$ interactions among three porphyrin $\pi$-planes of $TPZn_3$ and $\pi$-sphere of $PyC_{60}$, together with intramolecular $\pi$-bond formation between the porphyrin radical cation and the neutral porphyrin in $TPZn_3^{\bullet+}$.

## Summary and Conclusions

The present study has demonstrated unequivocally the electronic communication among porphyrins in the novel tripod porphyrin $TPZn_3$. In the absence of guest molecules, the $\pi$-bonds are formed between porphyrin rings in the oxidized states. In the presence of fullerene derivatives bearing with the $\pi$-sphere ($PyC_{60}$), $TPZn_3$ captures $PyC_{60}$ inside the cavity of the tripod. Efficient photoinduced electron transfer from $TPZn_3$ to $PyC_{60}$ occurs in the supramolecular complex, whereas no electron transfer from MPZn to $PyC_{60}$ occurs under the same experimental conditions because of its smaller association constants with $PyC_{60}$. The present study provides an excellent opportunity to clarify the difference among trimer ($TPZn_3$), dimer ($DPZn_2$), and monomer (MPZn) porphyrins for photoinduced electron transfer in noncovalently linked electron donor−acceptor systems. The $\pi-\pi$ interaction plays an important role to construct efficient electron donor−acceptor systems by controlling their electron-transfer properties.

## Experimental Section

**Chemicals and Reagents.** Silica gel (Merck; 70−120 mm) was used for column chromatography. Analytical thin layer chromatography was performed using Merck 60 F254 silica gel (precoated sheets, 0.2 mm thick). Reactions were monitored by thin-layer chromatography, UV−vis spectroscopy, and MALDI/TOF mass spectrometry. 4-(Azidomethyl)-benzaldehyde was synthesized as already described.[50] The preparation of MPZn was described elsewhere.[27] Tris(2,2′-bipyridyl)ruthenium(III) hexafluorophosphate

(47) The electrochemical potentials are corrected by taking into account the Coulombic interaction term and the ion solvation energy based on the Born dielectric continuum model, according to the following equation; $\Delta G_{CS} = E_{ox} - E_{red} - (e^2/4\pi\epsilon_0)[1/(R_{DA}\epsilon_s) - \{1/(2r_D) + 1/(2r_A)\}(1/\epsilon_s - 1/\epsilon_p)]$, where $e$ is elementary charge and $\epsilon_0$ is vacuum permittivity. In the present case, $r_D$ and $r_A$ are radii of electron donor (3.5 Å) and electron acceptor (3.7 Å) and $R_{DA}$ is center-to-center donor−acceptor distance (6 Å). $\epsilon_s = 2.4$ and $\epsilon_p = 9.6$ represent the dielectric constant of toluene and *o*-dichlorobenzene/$CH_2Cl_2$.

(48) (a) Arnold, B. R.; Farid, S.; Goodman, J. L.; Gould, I. R. *J. Am. Chem. Soc.* **1996**, *118*, 5482. (b) Flamigni, L.; Wyrostek, D.; Voloshchuk, R.; Gryko, D. T. *Phys. Chem. Chem. Phys.* **2010**, *12*, 474.

(49) (a) Arbogast, J. W.; Darmanyan, A. P.; Foote, C. S.; Rubin, Y.; Diederich, F. N.; Alvarez, M. M.; Anz, S. J.; Whetten, R. L. *J. Phys. Chem.* **1991**, *95*, 11. (b) Hung, R. R.; Grabowski, J. J. *J. Phys. Chem.* **1991**, *95*, 6073. (c) Ziessel, R.; Allen, B. D.; Rewinska, D. B.; Harriman, A. *Chem.−Eur. J.* **2009**, *15*, 7382.

(50) (a) Barbe, J.-M.; Canard, G.; Brandès, S.; Guilard, R. *Eur. J. Org. Chem.* **2005**, *21*, 4601. (b) Felts, A. S.; Siegel, B. S.; Young, S. M.; Moth, C. W.; Lybrand, T. P.; Dannenberg, A. J.; Marnett, L. J.; Subbaramaiah, K. *J. Med. Chem.* **2008**, *51*, 4911.

*Scheme 5*

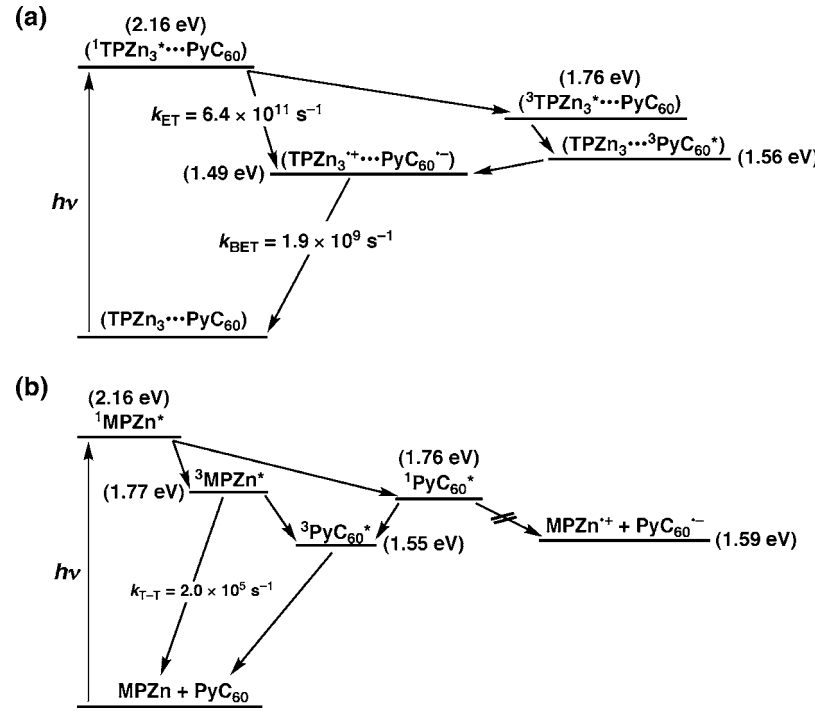


$[Ru(bpy)_3](PF_6)_3$ was prepared from tris(2,2′-bipyridyl)-ruthenium(II) chloride hexahydrate by the oxidation with $PbO_2$.[51] *N*-Methyl-2-(*p*-pyridyl)fulleropyrrolidine was prepared according to the literature.[52] Absolute dichloromethane ($CH_2Cl_2$: Carlo Erba) for synthesis, $CH_2Cl_2$ and toluene spectroscopic grade (Nacalai Tesque, Inc.) for analysis, $CS_2$ (Wako Pure Chemical Industries, Ltd.), *o*-dichlorobenzene and galvinoxyl free radical (Aldrich Chemical Co.), and 2-MeTHF (Tokyo Chemical Industry Co., Ltd.) were obtained commercially and used without further purification. Benzonitrile (PhCN) was purchased from Wako Pure Chemical Industries, Ltd., and distilled with $P_2O_5$ under reduced pressure.[53]

**Physicochemical Characterization of Compounds.** $^1$H NMR spectra were recorded on a Bruker Avance II 300 (300 MHz) or on a Bruker Avance DRX 500 (500 MHz) spectrometers at the "*Plateforme d'Analyse Chimique et de Synthèse Moléculaire de l'Université de Bourgogne (PACSMUB)*"; chemical shifts are expressed in ppm relative to chloroform (7.26 ppm) or pyridine (7.22, 7.58, and 8.74 ppm). UV−vis spectra were recorded on a Varian Cary 1 spectrophotometer. Mass spectra and accurate mass measurements (HR-MS) were obtained on a Bruker Daltonics Ultraflex II spectrometer in the MALDI/TOF reflectron mode using dithranol as a matrix or on a Bruker MicroQTof instrument in ESI mode. Both measurements were made at the "*Plateforme d'Analyse Chimique et de Synthèse Moléculaire de l'Université de Bourgogne (PACSMUB)*".

**Electrochemical Measurements.** Cyclic voltammetry (CV) measurements were carried out with a BAS 100W electrochemical analyzer in a deaerated solvent containing 0.10 M $TBAPF_6$ as a supporting electrolyte at 298 K. A conventional three-electrode cell was used with a platinum working electrode and a platinum wire as a counter electrode. The redox potentials were measured with respect to the $Ag/AgNO_3$ ($1.0 \times 10^{-2}$ M) reference electrode. The potential values (vs $Ag/AgNO_3$) are converted to those vs SCE by adding 0.29 V.[54]

**Photophysical Measurements.** UV−vis−NIR spectra were recorded on a Hewlett-Packard 8453 diode array spectrophotometer at various temperatures. Fluorescence and phosphorescence spectra were recorded on a Shimadzu spectrofluorophotometer (RF-5300PC). The fluorescence lifetimes of porphyrins were measured by a Photon Technology International GL-3300 with a Photon Technology International GL-302, nitrogen laser/pumped dye laser system, equipped with a four-channel digital delay/pulse generator (Stanford Research System Inc. DG535) and a motor driver (Photon Technology International MD-5020). The excitation wavelength was 415 nm.

**Laser Flash Photolysis Measurements.** Femtosecond transient absorption spectroscopy experiments were conducted using a Clark-MXR 2010 laser system and an optical detection system provided by Ultrafast Systems (Helios). The source for the pump and probe pulses was derived from the fundamental output of Integra-C (780 nm, 2 mJ/pulse and fwhm = 130 fs) at a repetition rate of 1 kHz. The pump beam was attenuated at 5 $\mu$J/pulse with a spot size of 1 mm diameter at the sample cell, where it was merged with the white probe pulse at a close angle (<10°). The probe beam, after passing through the 2 mm sample cell, was focused on a 200 $\mu$m fiber optic cable which was connected to a CCD spectrograph. Typically, 2500 excitation pulses were averaged to obtain the transient spectrum at a set delay time. Kinetic traces at appropriate wavelengths were assembled from the time-resolved spectral data. All measurements were recorded at 298 K.

Nanosecond time-resolved transient absorption measurements were carried out according to the following procedure. Experiments employed the pulses ($\lambda$ = 540 nm with the power of 2.5 mJ per pulse) from a Panther OPO pumped by a Nd:YAG laser (Continuum, SLII-10, 4−6 ns fwhm) at 298 K. The transient absorption spectra were monitored by continuous exposure to a xenon lamp (150 W) as a probe light and a photomultiplier tube (Hamamatsu 2949) as a detector. Toluene solutions containing porphyrins were prepared at concentrations such that the absorbance were around 0.4 at the excitation wavelength, and deoxygenated by argon purging for 10 min prior to use.

**Electron Spin Resonance (ESR) Measurements.** The ESR spectra were measured at various temperatures with a JEOL X-band spectrometer (JES-RE1XE). The ESR spectra were recorded under nonsaturating microwave power conditions. The magnitude of the modulation was chosen to optimize the resolution and the signal-to-noise (*S*/*N*) ratio of the observed spectra. The *g* values were calibrated

(51) Desimone, R. E.; Drago, R. S. *J. Am. Chem. Soc.* **1970**, *92*, 2343.
(52) Maggini, M.; Scorrano, G. *J. Am. Chem. Soc.* **1993**, *115*, 9798.
(53) *Purification of Laboratory Chemicals*, 5th ed.; Armarego, W. L. F., Chai, C. L. L., Eds.; Butterworth-Heinemann: Amsterdam, 2003.
(54) *Electrochemical Reactions in Nonaqueous Systems*; Mann, C. K., Barnes, K. K., Eds.; Marcel Dekker: New York, 1970.

with an $Mn^{2+}$ marker. $CH_2Cl_2$ solutions containing porphyrins were deaerated by argon purging for 10 min prior to use. The concentrations of radical species were qualitatively determined by double integration of the first-derivative ESR signal in reference to that of a known amount of a stable radical, galvinoxyl free radical, under the same experimental conditions. Since the radical concentration of the galvinoxyl radical is the same over the entire temperature range, variations of the ESR intensity only depend on the Curie law and instrumental factors such as cavity Q-factor. Thus, by comparing the ratio of the ESR intensity of $TPZn_3^{2+}$ ($I_P$) with that of galvinoxyl radical ($I_G$), the quantitative radical concentrations of $TPZn_3^{2+}$ can be determined at various temperatures.

**Theoretical Calculations.** Density-functional theory (DFT) calculations were performed on a COMPAQ DS20E computer. Geometry optimizations were carried out using the Becke3LYP functional and 3-21G(*) basis set with the Gaussian 03 program, revision C.02.[55] The graphical output of the optimized structure was generated with the Gauss View software program (version 3.09) developed by Semichem, Inc.[56]

**2,3,7,8,12,18-Hexamethyl-5-(4-azidomethylphenyl)-13,17-diethylporphyrin.** A mixture of 270 mg (1.68 mmol) of 4-(azidomethyl)-benzaldehyde and 1.00 g (1.67 mmol) of *a,c*-biladiene dihydrobromide was dissolved in 100 mL of hot absolute ethanol. *p*-Toluenesulfonic acid (1.7 g, 9.87 mmol) in 35 mL of ethanol was slowly added over 12 h, and the mixture was stirred under reflux for 48 h. The mixture was cooled to room temperature, and the solution was evaporated under vacuum. The residue was dissolved in dichloromethane (200 mL), neutralized with a saturated solution of $NaHCO_3$, and then washed thoroughly three times with 500 mL of water. The organic phase was dried over $MgSO_4$ and filtered, the solvent was removed in vacuo. The residue was purified by silica column chromatography ($CH_2Cl_2$/MeOH, 98/2). After crystallization from $CH_2Cl_2$/MeOH, the title compound was isolated in 23% yield (223 mg, 0.38 mmol) as a purple solid. $^1$H NMR ($CDCl_3$, 298 K): $\delta$ (ppm) = −3.31 (s, 2H, NH-imino), 1.89 (t, $J$ = 8.2 Hz, 6H, $CH_3$), 2.38 (s, 6H, $\beta$-$CH_3$), 3.50 (s, 6H, $\beta$-$CH_3$), 3.60 (s, 6H, $\beta$-$CH_3$), 4.04 (q, $J$ = 8.2 Hz, 4H, $CH_2$), 4.58 (s, 2H, $CH_2$−$N_3$), 7.56 (d, $J$ = 8.2 Hz, 2H, Ph), 7.96 (d, $J$ = 8.2 Hz, 2H, Ph), 9.91 (s, 1H, $H_{meso}$), 10.11 (s, 2H, $H_{meso}$). UV−vis ($CH_2Cl_2$): $\lambda_{max}$ (nm) ($\epsilon \times 10^{-3}$ $M^{-1}$ $cm^{-1}$) = 403.0 (341), 500.0 (16), 533.9 (13), 571.0 (12). HR-MS (MALDI/TOF): $m/z$ = 581.3225 $[M]^{\bullet+}$, 581.3267 calcd. for $C_{37}H_{39}N_7$.

**2,3,7,8,12,18-Hexamethyl-5-(4-azidomethylphenyl)-13,17-diethylporphyrinato-Zn (II).** 2,3,7,8,12,18-Hexamethyl-5-(4-azidomethylphenyl)-13,17-diethylporphyrin (200 mg, 0.352 mmol) and zinc acetate tetrahydrate (155 mg, 0.704 mmol, 2 equiv) were dissolved in chloroform (35 mL) and methanol (15 mL) and refluxed for 90 min in the presence of sodium acetate (289 mg, 3.25 mmol). The metalation reaction was monitored by UV−vis spectroscopy and MALDI/TOF mass spectrometry. At the end of the reaction, the solvent was removed under reduced pressure and the crude product was dissolved in $CH_2Cl_2$ (50 mL), washed with water (3 × 250 mL) and dried over $MgSO_4$. The solvent was removed in vacuo and the residue was purified by silica column chromatography ($CH_2Cl_2$ as eluent). After evaporation, the title compound was obtained in 91% yield (206 mg, 0.32 mmol) as a red microcrystalline solid. $^1$H NMR ($CDCl_3$, 298 K): $\delta$ (ppm) = 1.83 (t, $J$ = 7.4 Hz, 6H, $CH_3$), 2.40 (s, 6H, $\beta$-$CH_3$), 3.48 (s, 6H, $\beta$-$CH_3$), 3.57 (s, 6H, $\beta$-$CH_3$), 4.01 (q, $J$ = 7.4 Hz, 4H, $CH_3$−$CH_2$), 4.67 (s, 2H, $CH_2$−$N_3$), 7.66 (d, $J$ = 8.0 Hz, 2H, Ph), 8.05 (d, $J$ = 8.0 Hz, 2H, Ph), 9.89 (s, 1H, $H_{meso}$), 10.04 (s, 2H, $H_{meso}$). UV−vis ($CH_2Cl_2$): $\lambda_{max}$ (nm) ($\epsilon \times 10^{-3}$ $M^{-1}$ $cm^{-1}$) = 404.0 (215), 534.0 (11), 570.0 (10). HR-MS (MALDI/TOF): $m/z$ = 643.2416 $[M]^{\bullet+}$, 643.2402 calcd. for $C_{37}H_{37}N_7Zn$.

**Diporphyrin Biszinc $DPZn_2$.** 2,3,7,8,12,18-Hexamethyl-5-(4-azidomethylphenyl)-13,17-diethylporphyrin (31 mg, 48.2 $\mu$mol) and 5-(4-ethynylphenyl)-13,17-diethyl-2,3,7,8,12,18-hexamethylporphyrin zinc (30 mg, 49.1 $\mu$mol) were dissolved in 15 mL of THF in a 100 mL round-bottom flask fitted with a reflux condenser. Sodium ascorbate (15.7 mg, 79 $\mu$mol) dissolved in 1 mL of water and $CuSO_4 \cdot 5H_2O$ (6.7 mg, 30 $\mu$mol) were added to the solution. The reaction mixture was stirred at 70 °C for 64 h. The solution was then evaporated under reduced pressure and dissolved in 30 mL of methylene chloride. The solution was washed twice with a saturated $NH_4Cl$ solution then dried over anhydrous $MgSO_4$. After filtration over a silica plug ($CH_2Cl_2$/Heptane, 50/50), the unreacted reagents were eliminated. Further purification by silica gel chromatography (first $CH_2Cl_2$ then $CH_2Cl_2$/MeOH, 96/4) afforded the title compound in 43% yield (26 mg, 20.6 $\mu$mol) as a purple solid. $^1$H NMR (Pyridine-$D_5$, 298 K): $\delta$ (ppm) = 1.79 (t, $J$ = 7.5 Hz, 12H, $CH_3$), 2.50 (m, 12H, $CH_3$), 3.48 (m, 24H, $CH_3$), 4.04 (q, $J$ = 7.5 Hz, 8H, $CH_2$), 6.15 (s, 2H, $CH_2$−Ar), 7.77 (d, $J$ = 7.8 Hz, 2H, $H_{Ar}$), 8.12 (d, $J$ = 7.8 Hz, 2H, $H_{Ar}$), 8.25 (d, $J$ = 7.8 Hz, 2H, $H_{Ar}$), 8.61 (d, $J$ = 7.8 Hz, 2H, $H_{Ar}$), 8.83 (s, 1H, $H_{triazole}$), 10.32 (s, 2H, $H_{meso}$), 10.39 (s, 4H, $H_{meso}$). UV−vis ($CH_2Cl_2$): $\lambda_{max}$ (nm) ($\epsilon \times 10^{-3}$ $M^{-1}$ $cm^{-1}$) = 405.0 (420), 535.0 (21), 571.0 (19.5). MS (MALDI/TOF): $m/z$ = 1255.43 $[M]^{\bullet+}$, 1255.46 calcd. for $C_{75}H_{73}N_{11}Zn_2$. HR-MS (ESI): $m/z$ = 1255.4410 $[M]^{\bullet+}$, 1255.4633 calcd. for $C_{75}H_{73}N_{11}Zn_2$; $m/z$ = 1278.4461 $[M+Na]^+$, 1278.4531 calcd. for $C_{75}H_{73}N_{11}NaZn_2$.

**Trisporphyrin Triszinc $TPZn_3$.** 2,3,7,8,12,18-Hexamethyl-5-(4-azidomethylphenyl)-13,17-diethylporphyrin (45 mg, 66 $\mu$mol, 3 equiv) and tripropargylamine (2.91 mg, 22.2 $\mu$mol) were dissolved in 15 mL of THF in a 100 mL round-bottom flask fitted with a reflux condenser. Sodium ascorbate (43.9 mg, 222 $\mu$mol, 10 equiv) dissolved in 1 mL of water and $CuSO_4 \cdot 5H_2O$ (22.2 mg, 111 $\mu$mol, 5 equiv) were added to the solution. The reaction mixture was stirred at 70 °C for 48 h. The solution was then evaporated under reduced pressure and dissolved in 30 mL of methylene chloride. The solution was washed twice with a saturated $NH_4Cl$ solution then dried over anhydrous $MgSO_4$. After purification over a silica plug ($CH_2Cl_2$/Heptane, 50/50), the unreacted reagents were eliminated. Further purification by silica gel chromatography (first $CH_2Cl_2$ then $CH_2Cl_2$/MeOH, 95/5) afforded the title compound in 29% yield (13 mg, 6.3 $\mu$mol) as a purple solid. $^1$H NMR ($CDCl_3$, 298 K): $\delta$ (ppm) = 1.67 (t, $J$ = 8.3 Hz, 18H, $CH_3$), 1.96 (s, 18H, $\beta$-$CH_3$), 3.08 (s, 18H, $\beta$-$CH_3$), 3.29 (s, 18H, $\beta$-$CH_3$), 3.74 (q, $J$ = 8.3 Hz, 12H, $CH_2$), 4.10 (s, 6H, N−$CH_2$-Triazole), 5.88 (s, 6H, Ph−$CH_2$-Triazole), 7.42 (m, 12H, Ph), 8.06 (s, 3H, $H_{triazole}$), 9.32 (s, 3H, $H_{meso}$), 9.39 (s, 6H, $H_{meso}$). UV−vis ($CH_2Cl_2$): $\lambda_{max}$ (nm) ($\epsilon \times 10^{-3}$ $M^{-1}$ $cm^{-1}$) = 404.9 (375), 537.0 (26), 571.9 (24). MS (MALDI/TOF): $m/z$ = 2061.15 $[M]^{\bullet+}$, 2060.79 calcd. for $C_{120}H_{121}N_{22}Zn_3$. HR-MS (ESI): $m/z$ = 2083.7860 $[M+Na]^+$, $m/z$ = 1041.8950 $[M+Na]^{2+}$ calcd. for $C_{120}H_{120}N_{22}Na_1Zn_3$: 2083.7838 (monocation), 1041.8913 (dication).

**Acknowledgment.** This research was supported by KOSEF/MEST through WCU project (R31-2008-000-10010-0) and Grants-in-Aid (No. 20108010) from the Ministry of Education, Culture, Sports, Science and Technology, Japan. A.T. appreciates support from the Global COE program "Global Education and Research Center for Bio-Environmental Chemistry" of Osaka University (S.F.) and JSPS fellowship for young scientists. The Centre National de Recherche Scientifique (CNRS, UMR 5260) and "Région Bourgogne" are also acknowledged for funding.

**Supporting Information Available:** ESI HR-MS spectrum of $TPZn_3$ (S1), $^1$H NMR spectrum of $TPZn_3$ (S2), cyclic voltammograms of MPZn, $DPZn_2$, and $TPZn_3$ in PhCN (S3), vis−NIR spectral changes upon addition of $[Ru(bpy)_3]^{3+}$ to a $CH_2Cl_2$ solution of MPZn and $DPZn_2$ (S4), vis−NIR spectral changes

(55) Frisch, M. J.; *Gaussian 03, Revision C.02*; Gaussian, Inc.: Wallingford, CT, 2004. The full list of authors is given in the Supporting Information.

(56) Dennington R., II; Keith, T.; Millam, J.; Eppinnett, K.; Hovell, W. L.; Gilliland, R. *Gauss View*, version 3.09; Semichem, Inc.: Shawnee Mission, KS, 2003.

upon addition of $[Ru(bpy)_3]^{3+}$ (3−6 equiv) to a $CH_2Cl_2$ solution of $TPZn_3$ (S5), ESR spectra of $TPZn_3$ in the presence of $[Ru(bpy)_3]^{3+}$ and dependence of the ESR intensity ($I_{ESR}$) on the ratio of concentration of $[Ru(bpy)_3]^{3+}$ to $TPZn_3$ (S6), Molecular orbital diagrams for the radical cation and the radical cation dimer (S7), $^1$H NMR spectra of $TPZn_3$ and MPZn in the absence and presence of $C_{60}$ (S8), Job's plot for the complexation between $TPZn_3$ and $PyC_{60}$ in *o*-dichlorobenzene (S9), Fluorescence spectral changes of $TPZn_3$ upon addition of $PyC_{60}$ and change in the fluorescence intensity at 577 nm (S10), $^1$H NMR spectra of $PyC_{60}$ and MPZn in the absence and presence of $PyC_{60}$ for the determination of association constant between MPZn and $PyC_{60}$ (S11), cyclic voltammograms of $TPZn_3$ in the absence and presence of $PyC_{60}$ (S12), and full author list of ref 55 (S13). This material is available free of charge via the Internet at http://pubs.acs.org.

JA100192X